The Thesis committee for Khai Ta Nguyen

Certifies that this is the approved version of the following thesis:

Thermal Characterization of InAs Interfacial Misfit Arrays Using Nanosecond Thermoreflectance Method

APPROVED BY SUPERVISING COMMITTEE:

Supervisor: _____

Yaguo Wang

_____

Vaibhav Bahadur

Thermal Characterization of InAs Interfacial Misfit Arrays Using Nanosecond Thermoreflectance Method

by

Khai Ta Nguyen, B.S.M.E.

Thesis

Presented to the Faculty of the Graduate School

of the University of Texas at Austin

in Partial Fulfillment

of the Requirements

for the Degree of

Master of Science in Engineering

The University of Texas at Austin

May 2015

Acknowledgements

First, I would like to thank Dr. Yaguo Wang with her guidance and patience, for which this thesis would have not been possible. I would also like to thank Dr. Seth Bank and his group, especially Daniel Ironside, for providing samples for my thermoreflectance setup in order for their thermal properties to be measured. Special thanks would have to go to my past and present group members, Feng He, Xianghei Meng, Jihoon Jeong, Dr. Ke Chen, and Dr. Wenzhi Wu, who have supported me with their technical expertise in developing my system. I also would like to thank Dr. Yildiz Bayazitoglu from Rice University for inspiring me to specialize in thermal-fluid systems for my master's degree and helping me in the graduate school application process. I also would like to give thanks to my students who had me as a teaching assistant in both the Heat Transfer and Experimental Heat Transfer courses. I enjoyed teaching all of you.

Finally, I would like to thank my parents for raising me to the person that I am today, my two older brothers for helping me through my struggles, and my grandfather for teaching and taking care of me since I was a toddler.

Thermal Characterization of InAs Interfacial Misfit Arrays Using Nanosecond Thermoreflectance Method

by

Khai Ta Nguyen, M.S.E.

The University of Texas at Austin, 2015

SUPERVISOR: Yaguo Wang

Abstract

Thermal properties are of the utmost importance because of the ever growing demands given to us by high-power and ultrafast electronics. A nanosecond thermoreflectance method was developed to determine the thermal conductivities of InAs interfacial misfit arrays (IMF). These interfacial misfit arrays were designed to improve the optical properties, such as photoluminescence, of these materials in order to improve electronic devices. A study was performed to see if the thermal properties of these materials were affected in any way. The nanosecond thermoreflectance method was benchmarked with control samples of InAs and GaAs substrates, and the thermal conductivities were close to that of bulk value. After performing the experiments, it was found that the thermal conductivity varies inversely with photoluminescence. It was also found that the thermal interface resistance between the growth and the substrate was inversely proportional to the thickness of the IMF growth.

Table of Contents

List of Tables.

List of Figures

.

Chapter One: Introduction and Background

1.1 Introduction and Background

The purpose of this thesis is to develop and implement a nanosecond thermoreflectance method to determine the thermal properties, mainly thermal conductivity, for novel materials. The first part of this thesis will be devoted to the theory and background behind this technique. The second part of this thesis will be devoted to validity of this nanosecond thermoreflectance system. The third part will be devoted to a case study involving semiconductor interface misfit arrays.

Today's technology has been advancing ever so quickly. In field of electronics, the new devices are quickly becoming faster and more powerful while maintaining characteristic lengths on the scale of micrometers and nanometers. However, with this shift going towards smaller devices, a challenge arises from trying to maintain the proper temperature of these devices (Schelling, 2005).

Because of the smaller length scales and the increasing power output, temperatures of these devices can become high if not managed properly. High temperature for these devices can cause thermal stress, which can lead to decreased device lifetimes and mechanical failure. Therefore, the thermal properties of these devices must be taken into account. However, the thermal conductivity for these materials on these small length scales do not match of those of bulk materials. These different thermal conductivity values on the smaller length scales can be attributed to multiple factors, such as microstructural differences and phonon transport mechanisms.

Thus, the thermal conductivities must be measured to find these differences from the bulk values.

There are two types of methods that can be used to measure thermal conductivity of materials: steady-state and transient.

The most commonly used steady state method is the steady state bar method. The sample is placed between two plates. One plate is being heated by steam while the other plate is being cooled with cold water. This is used in order to create a temperature gradient across the sample. We can relate the thermal conductivity for this case to the temperature field, governed by Fourier's law:

$$q'' = k\frac{\partial T}{\partial x} \tag{1}$$

where $q''$is the heat flux, k is the thermal conductivity, and $\frac{\partial T}{\partial x}$ is the temperature difference over the length of the sample. With the heat flux known, the thermal conductivity can be determined. However, the time it takes for all of the experimental parameters to reach steady state is long, and the experiment must be performed in a vacuum. Thus, these steady state methods are not viable for today's topics.

Because the steady state method can take a long time, transient methods were developed to speed up the process. One such method is the laser flash method. This method uses a laser pulse incidented onto the front surface of the sample while the temperature of the rear surface of the sample is measured with respect to time using a thermocouple. The experimental parameters are designed to ensure 1-D heat conduction

and it was found that the temperature distribution of the sample in question can be given with the following equaton.

$$T(L,t) = \frac{Q}{\rho c L}\left[1 + 2\sum_{n=1}^{\infty}(-1)^n \exp\left(-\frac{n^2\pi^2}{L^2}\alpha t\right)\right] \quad (2)$$

where Q is the pulse energy, ρ is the density of the material, c is the specific heat, and α is the thermal diffusivity. The thermal conductivity can be extracted from the this equation from the thermal diffusivity, which is given by:

$$\alpha = \frac{k}{\rho c} \quad (3)$$

where k is the thermal conducitivity.

1.2 Thermoreflectance Method

The method that will be used for this thesis is the thermoreflectance method. For this method, a laser pulse is irradiated on a sample surface in order to induce a change in the surface reflectivity. It has been noted that small changes in the surface reflectivity is linearly proportional to small changes in temperature. We then can extract thermal properties from data generated by this phenomenon.

At its simplest explanation, the thermoreflectance model uses two beam paths: a pump beam path and a probe beam path. The pump beam path acts as the heat source for the sample and has an output power usually on the scale of milliwatts. The probe beam path is used as a sensor, which can detect changes in the reflectivity of the sample before and after the pump pulse strikes the sample. The two beam paths have to overlap spatially on the sample, or else, no changes in reflectivity can be detected. Since the intensity of a

pulse hitting the surface decays over the time, there must be a delay between the pump and probe paths hitting the sample in order to measure the reflectivity change.

The thermoreflectance method can be performed with pulse widths of multiple time scales. One such experimental setup uses two laser sources producing pulses with pulse widths on the scale of femtoseconds. The transient part of the reflectivity change is measured using a motorized delay stage in order to change the distance between the pump and probe pulses hitting the surface. The probe beam after hitting the surface of the sample goes through a series of optical elements before entering a photodetector which converts optical signals into electrical signals.

Another experimental setup uses laser pulses with widths on the scale of picoseconds with the pump pulse hitting the rear side of the sample while the probe pulse hits the front side of the sample. This particular method works similarly to the laser flash method, as mentioned before, but on a much faster time scale. These experimental setups can be used to detect other material properties besides thermal conductivities.

The simplest setup, which is used for the purpose of the thesis, using this method involves a nanosecond pump laser to heat the surface of the sample in conjunction with a continuous waveform laser to probe the sample. A balanced detector and oscilloscope is used to extract the data from the system. A normalized signal change is mapped to a temperature profile, which we can extract the thermal conductivity from this data. Unlike other thermoreflectance methods which use pump pulse widths on the scale of femtoseconds and picoseconds, a thermoreflectance method using a nanosecond laser pump pulse does not contain any coupled oscillations. This is due to the lifetimes of the

coherent phonons in relation to time resolution detected by the probe laser. Since coherent phonon lifetimes are on the scale of picoseconds, it is impossible to see these coupled oscillations associated with these coherent phonons. Thus, the thermal conductivity and thermal contact resistance can extracted from the data without worrying about any noise effects from the data. More information about this experimental setup will be discussed in chapter two.

1.3 Organization

This section discusses the various methods of measuring thermal conductivity of different materials. The first methods were steady-state that involved finding the temperature distribution of a solid slab. Because steady-state methods take a long time to output any results, transient methods were developed, starting with the laser flash method and improving till the thermoreflectance method was developed. The thermoreflectance method is useful in determining thermal properties as well as other optical properties, such as phonon lifetime and frequency. The second chapter of this thesis will go into further detail of the thermoreflectance method setup that was used in the experiments as well as the finite difference thermal model used to determine the thermal conductivity. The third chapter will look at a case study of interfacial misfit arrays and their thermal properties. The fourth chapter will summarize the thesis and state future work that will be done.

Chapter Two: Thermoreflectance Method

2.1 Experimental Setup

The schematic of the experimental setup is shown below in Figure 1.

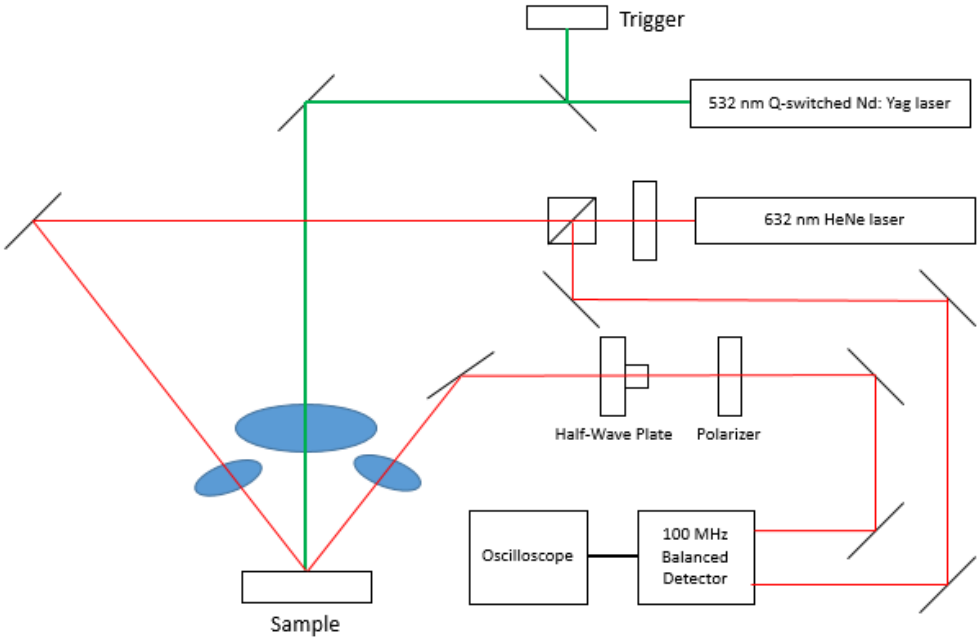

Figure 16. **Experimental Setup used for Thermoreflectance Method.**

There are two laser sources used in this setup. The Q-switched 532 nm laser is used as the heat source for the sample. The pulse width of the 532 nm laser depends on the current inputted in the source. For this case, a 4.0 Ampere current was used, which corresponds to a 25-ns pulse width.

The other laser used in the setup is a 632 nm continuous-wave laser. The intensity of the probe laser is first monitored by using a continuous ND filter. A 50-50 cube beam splitter is then used to split the probe beam into two paths. One path is used as a reference for a benchmark. The other path is reflected off the sample and into the detector to

determine the changes in reflectivity due to the pump beam. The balanced detector has a bandwidth of 100 MHz (10 ns rise time) and a gain of $50 * 10^3$ V/A.

The spot sizes of the both lasers are measured using the knife-edge test (Magnes 2006). The knife edge test is useful for determining the radius of the beam spots at certain points along the optical system. Since the shape of the laser pulses are Gaussian shaped, the radius of the beam spots can be determined by the intensity of the laser pulse, according to the shape of the pulse. It was found that the beam spot for the pump beam is 0.2966 mm and the beam spot size for the probe beam is 0.08477 mm.

The fluence of the pump beam is chosen, such that it gives a reasonable signal-to-noise ratio and the temperature change is still in the linear region. Figure 2 shows the relationship between the input current and peak intensity of the pump pulse.

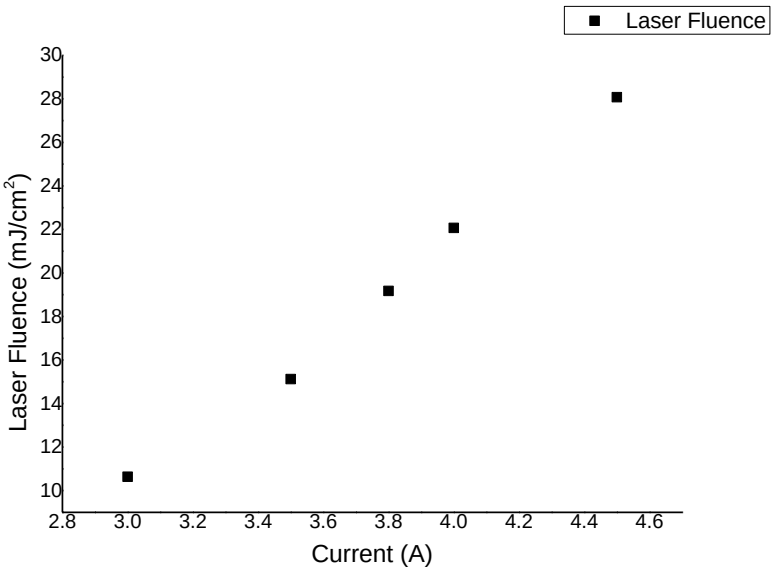

Figure 17. Laser Fluence vs. Current plot

For the experiments used in this thesis, a 4.0 Ampere current was used for the pump laser source.

An experiment was performed to check for the validity of the relationship between the surface temperature and the surface reflectivity. The experimental setup is shown below in Figure 3.

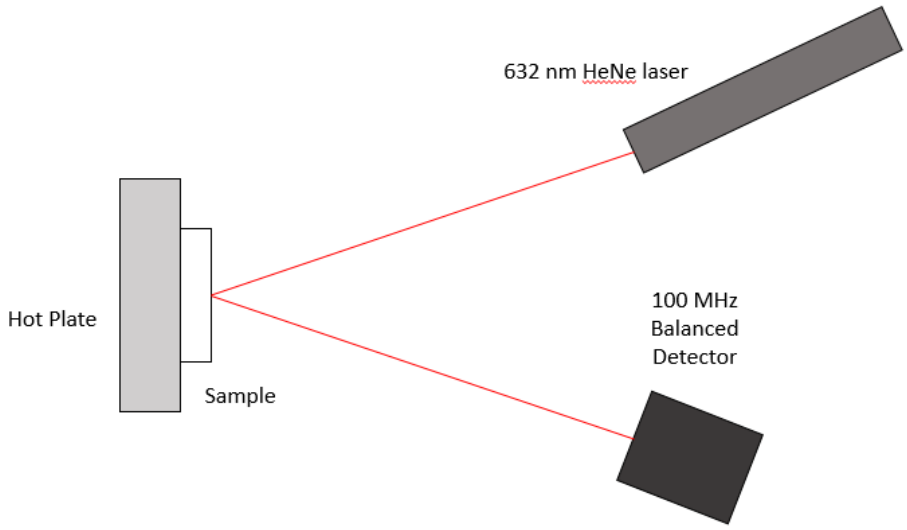

Figure 18. Experimental Setup for Reflectivity vs. Temperature Measurements.

For this experiment, a silicon sample coated in 70 nm Au thin film is placed on the side of a hot plate with thermal glue on the rear surface to keep the sample from falling off. The 632 continuous-waveform laser was used for this experiment. The reference mean voltage was taken first without irradiating onto the sample surface to use as a basis to compare to the reflectivity changes once the sample is heated. Then, the mean voltage was then recorded for each temperature point on the rear surface. In order to get the true surface temperature, a thermocouple was placed on the surface and the

difference between the temperature of the hot plate and the temperature of the surface was noted. The lowest temperature was used as the reference temperature for normalization. The reflectivity vs. temperature graph and the normalized reflectivity vs. temperature graph are shown in Figures 4 and 5, respectively.

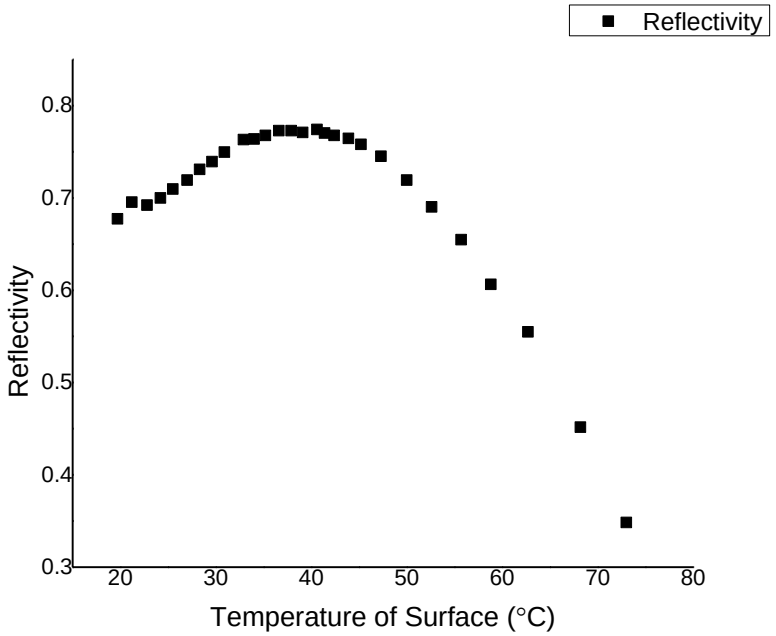

Figure 19. Reflectivity vs. Temperature plot

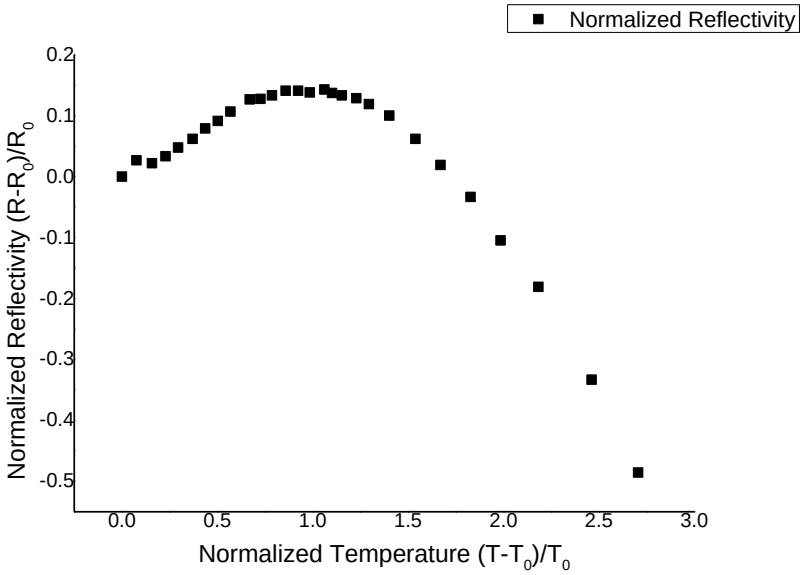

Figure 20. Normalized Reflectivity vs. Normalized Temperature plot.

From Figures 4 and 5, it appears that our linear relationship between the changes in the reflectivity and temperature is valid for a certain temperature region of 20-35℃. Because our thermoreflectance experiment starts operating at room temperature, the linear region will be sufficient enough for our experiment.

2.2 Thermal Finite Difference Model

The model that will be used to fit the data is the one-dimensional transient heat conduction equation with heat generation. The equation used is as followed:

$$\rho c_p \left(\frac{\delta T}{\delta x}\right) = k \frac{\delta^2 T}{\delta x^2} + S(x,t) \qquad (4)$$

where ρ is the density of the material, c_p is the specific heat, and S is the source term, due to the pump laser pulse. We can assume this to be one-dimensional because of the ratios of the spot sizes of the pump and probe laser. The intensity of the pump laser has a Gaussian shape with respect to the radius from the center. If the radius of the probe laser

is significantly less than the radius of the pump laser, then the intensity of the pump laser probed by the probe laser is near uniform with respect to distance from the center if the centers of both the pump and probe laser overlap perfectly. Thus, we can assume the intensity of the source term is not a function of the radius from the center.

The source term equation is given as Beer-Lambert's Law:

$$S(x,t) = S_0(1-R)\alpha' \exp(-\alpha' x) \exp\left(\left(\frac{t}{t_p}\right)^2\right) \quad (5)$$

where S_0 is the maximum volumetric power generation, R is the reflectivity of the sample surface, α' is the absorption coefficient, and t_p is the pulse width of the pump laser. The absorption coefficient is determined by the properties of both the pump laser and the surface layer and is given by the following equation:

$$\alpha = \frac{\lambda}{4\pi k'} \quad (6)$$

where λ is the wavelength of the pump laser and k' is the imaginary coefficient of the surface layer.

In order to simplify the model, we assume the first layer absorbs all of the heat, provided by the pump laser. Thus, for the model, the source term only applies for the first layer, and it disappears for any subsequent layers. From a physical standpoint, it is due to the electrons in the film/first layer absorbing the laser irradiation and transferring energy to the lattice. Once thermal equilibrium is reached, the thermal energy is then diffused through the whole sample.

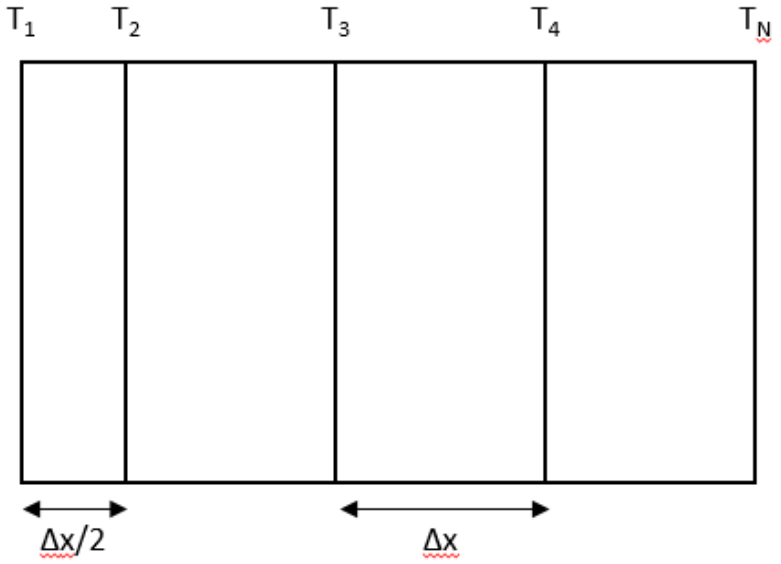

Figure 21. Nodal system for use in thermal model.

Because the source term makes this model difficult to solve by analytical means, a numerical model must be used for this case. An implicit finite difference method is used to model the thermoreflectance experiment. An energy balance is performed on an differential element of thickness Δx on an interior nodal point, using the following equation:

$$\frac{\delta \dot{E_{st}}}{\delta t} = \dot{E_{in}} - \dot{E_{out}} + \dot{E_{gen}} \tag{7}$$

Using a thermal resistance network, we can map the transfer of thermal energy from one nodal point to the next.

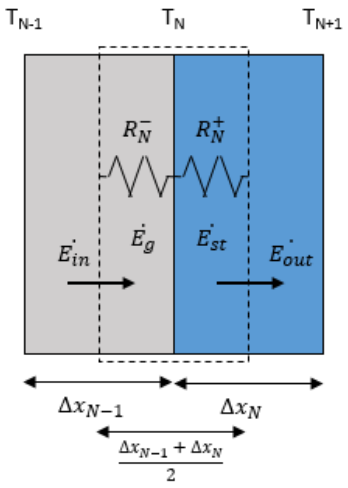

Figure 22. Schematic of finite control volume with appropriate resistances and energy terms.

By performing an energy balance on the control in our nodal resistance network, we can determine the temperature at each nodal point at any given time step. We use the following equations for the resistances:

$$R_N^+ = \frac{\Delta x_N}{2k_N} \tag{8a}$$

$$R_N^- = \frac{\Delta x_N}{2k_N} \tag{8b}$$

where k_n is the thermal conductivity at space point N. Using these resistance equations, we can plug into the each energy term to get our full energy balance equation in terms of the temperature points and resistances.

$$\dot{E}_{in} = \frac{T_{N-1} - T_N}{R_{N-1}^+ + R_N^-} \tag{9a}$$

$$\dot{E}_{out} = \frac{T_{N-1} - T_N}{R_{N-1}^+ + R_N^-} \tag{10}$$

$$\dot{E}_{gen} = \frac{S_{N-1} + S_N}{2} \tag{11}$$

$$\dot{E}_{st} = \rho c_p T \frac{\Delta x_{N-1} + \Delta x_N}{2} \tag{12}$$

We can then use an implicit difference method scheme to set up our model. Plugging in the terms for our energy terms, we get the following equation at time step *i* and spatial step *N*:

$$(\rho c_p)_N \frac{T_N^{i+1} - T_N^i}{\Delta t} * \frac{\Delta x_{N-1} + \Delta x_N}{2} = \frac{T_{N-1}^{i+1} - T_N^{i+1}}{R_{N-1}^+ + R_N^-} - \frac{T_N^{i+1} - T_{N+1}^{i+1}}{R_N^+ + R_{N+1}^-} + \frac{S_{N-1}^i + S_N^i}{2} \tag{13}$$

This equation serves as the basis of our implicit difference method scheme in order to find the temperature profile spatially at each time step *I* and the temperature profile of the surface at the first spatial step with respect to time.

This equation is then nondimensionalized to help with the computation and fitting process. The values in the equation can range on the order of multiple magnitudes, so by nondimensionalizing the terms, we can put the whole equation on roughly the same order of magnitude. The following nondimensionalized terms are used for this equation:

$$x^* = \frac{x}{x_0} \tag{14}$$

$$t^* = \frac{t}{t_0} \tag{15}$$

$$R^* = \frac{k_0}{x_0} R \tag{16}$$

$$\left(\rho c_p\right)^* = \frac{(\rho c_p)}{(\rho c_p)_0} \tag{17}$$

$$\theta = \frac{T - T_\infty}{T_\infty} \tag{18}$$

where any term with a * as the superscript is the nondimensionalized term, any term with a 0 as the subscript is the reference term, and T_∞ is room temperature. The θ

term tracks the normalized change in temperature and serves as the basis of our fitting process, which we can use to find the thermal conductivity of our sample.

Once the nondimensionalized terms are formulated, they are plugged into the equation. The terms are then rearranged in with respect to the normalized temperature terms and formulated in the following way:

$$\theta_{N-1}^{i+1}\left[-\frac{Fo}{R_{N-1}^{+*}+R_N^{-*}}\right]+\theta_N^{i+1}\left[\frac{(\rho c_p)_N^{*}(\Delta x_{N-1}^{*}+\Delta x_N^{*})}{2\Delta t^{*}}+\frac{Fo}{R_{N-1}^{+*}+R_N^{-*}}+\frac{Fo}{R_N^{+*}+R_{N+1}^{-*}}\right]+\theta_{N-1}^{i+1}\left[-\frac{Fo}{R_N^{+*}+R_{N+1}^{-*}}\right]=$$

$$\theta_N^{i}\left[\frac{(\rho c_p)_N^{*}(\Delta x_{N-1}^{*}+\Delta x_N^{*})}{2\Delta t^{*}}\right]+\frac{t_0}{T_\infty x_0(\rho c_p)_0}\frac{S_{N-1}^{i}+S_N^{i}}{2} \tag{19}$$

where *Fo* is the reference Fourier number defined by:

$$Fo=\frac{k_0 t_0}{{x_0}^2(\rho c_p)_0} \tag{20}$$

Equation (#) can be simplified into a system of equations. By redefining the coefficients of the normalized temperature, equation (#) can be arranged into a tridiagonal matrix in the form of:

$$A_N\theta_{N-1}^{i+1}+B_N\theta_N^{i+1}+C_N\theta_{N+1}^{i+1}=D_N \tag{21}$$

where the coefficients are defined as followed:

$$A_N=-\frac{Fo}{R_{N-1}^{+*}+R_N^{-*}} \tag{22a}$$

$$B_N=\frac{(\rho c_p)_N^{*}(\Delta x_{N-1}^{*}+\Delta x_N^{*})}{2\Delta t^{*}}+\frac{Fo}{R_{N-1}^{+*}+R_N^{-*}}+\frac{Fo}{R_N^{+*}+R_{N+1}^{-*}} \tag{22b}$$

$$C_N=-\frac{Fo}{R_N^{+*}+R_{N+1}^{-*}} \tag{22c}$$

$$D_N=\theta_N^{i}\left[\frac{(\rho c_p)_N^{*}(\Delta x_{N-1}^{*}+\Delta x_N^{*})}{2\Delta t^{*}}\right]+\frac{t_0}{T_\infty x_0(\rho c_p)_0}\frac{S_{N-1}^{i}+S_N^{i}}{2} \tag{22d}$$

The A, B, and C coefficients form a tri-diagonal matrix, which can be inverted to find the temperature profile at time step *i+1*. The calculated temperature from this inversion at time step *i+1* then replaces the temperature at time step *i*, and the process is repeated for each subsequent time step. For the D coefficients, any nodal points that are not in the first layer will not contain any source terms, and the coefficients are then rewritten as such for any N greater than the length of the first layer divided by Δx:

$$D_N = \theta_N^i \left[\frac{(\rho c_p)_N^* (\Delta x_{N-1}^* + \Delta x_N^*)}{2\Delta t^*} \right] \tag{23}$$

There are two special cases for this model where the coefficients must be modified for the model to be accurate. One case is at the first nodal point on the surface. The other case is at an interface point between two dissimilar materials.

The first case will be for the first nodal point on the surface. At this nodal point, the differential volume element will have a length of Δx/2 rather than Δx. The reason for this modification to the model will be explained later for the second case of the interface between two dissimilar materials.

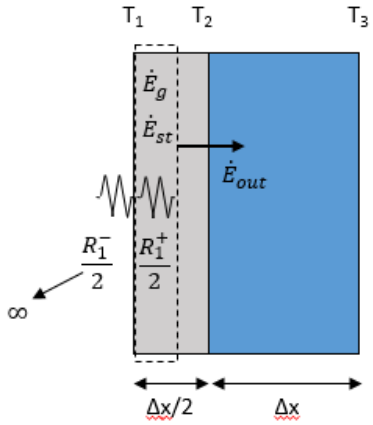

Figure 23. Schematic for finite control volume for first nodal point.

We can think of this first nodal point as an interface between two different materials in terms of our resistance network. The resistance element to the left of the nodal point will be air while the resistance element to the right of the nodal point will be the first layer. Because the thermal conductivity of air at room temperature (25 °C) and normal atmospheric pressure is 0.02551 $\frac{W}{m-K}$, the resistance terms will approach infinity. Thus, the coefficients for the first nodal point are as followed:

$$A_1 = 0 \tag{24a}$$

$$B_1 = \frac{(\rho c_p)_1^*(\Delta x_N^*)}{2\Delta t^*} + \frac{Fo}{\frac{R_1^{+*}}{2}+\frac{R_2^{-*}}{2}} \tag{24b}$$

$$C_1 = -\frac{Fo}{\frac{R_1^{+*}}{2}+\frac{R_2^{-*}}{2}} \tag{24c}$$

$$D_1 = \theta_1^i\left[\frac{(\rho c_p)_1^*(\Delta x_1^*)}{2\Delta t^*}\right] + \frac{t_0}{T_\infty x_0(\rho c_p)_0}\frac{S_1^i}{2} \tag{24d}$$

The A_1 coefficient becomes zero for this nodal point, which helps in formulating the ABC matrix.

The second case is at an interface point between two dissimilar materials. When two materials meet at an interface, there is usually a temperature drop between the two surfaces where they contact. This temperature drop is due to the interfacial thermal resistance. Ideally, when two materials come into contact, their surfaces are so smooth that all points on the surface come into contact with one another. However, this ideal case is rare, as there will be air gaps between these surfaces, and an additional interface thermal resistance term must be taken into account.

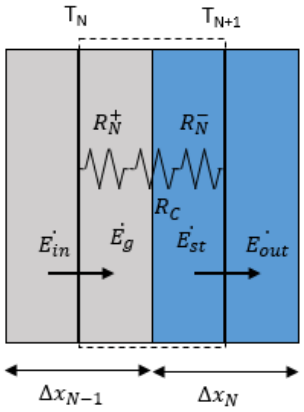

Figure 24. Schematic for finite control volume at an interface point between two dissimilar materials.

Because of the temperature discontinuity at the interface, it is impossible to place a single nodal point there. There are two solutions to this problem. One solution would be to place two nodes at the interface to account for temperature discontinuity there. Another solution would be to shift the nodal system Δx/2 into the sample, such that there is no nodal point on the interface. The second solution was used for this model. Because this model was shifted in by Δx/2, an additional nodal point must be placed on the surface.

That is why the control volume at the first nodal point is half the size as the rest of the control volumes.

The matrix coefficients that change as a result of this interface are shown below. The notation for this interface point is from Figure 9.

$$B_N = \frac{\left(\rho c_p\right)_N^* (\Delta x_{N-1}^* + \Delta x_N^*)}{2\Delta t^*} + \frac{Fo}{R_{N-1}^{+*} + R_N^{-*}} + \frac{Fo}{R_N^{+*} + R_C + R_{N+1}^{-*}} \tag{25a}$$

$$C_N = -\frac{Fo}{R_N^{+*} + R_C + R_{N+1}^{-*}} \tag{25b}$$

$$B_{N+1} = -\frac{Fo}{R_N^{+*} + R_C + R_{N+1}^{-*}} \tag{25c}$$

$$C_{N+1} = \frac{\left(\rho c_p\right)_N^* (\Delta x_N^* + \Delta x_{N+1}^*)}{2\Delta t^*} + \frac{Fo}{R_{N+1}^{+*} + R_{N+2}^{-*}} + \frac{Fo}{R_N^{+*} + R_C + R_{N+1}^{-*}} \tag{25d}$$

As noted from the equations above, the B and C values change as a result of the additional interface resistance term. This interface resistance term will play a big part in our experimental procedure.

One thing before moving on to the actual experiments must be noted: our choice of the step size Δx. Our choice of the step size is governed by the thickness of each layer in order to get an accurate measurement. Thus, the thinnest layer helps us choose our step size. For the samples that will be discussed later, the thinnest layer (a gold metal film) has a length of 70 nm, so our choice of step size would be 10 nm. This choice of Δx will be problematic when performing the simulations to find the thermal conductivity. Besides the gold metal film, there are layers that are 400-800 nm thick and substrates that are 0.5 mm thick. This poses a challenge computationally, as primarily using a step size of 10 nm will cause our ABC matrix to be very large. Because our matrix is very large, it will

take a long time to compute the best fit for a given data set. A single fitting can take up to 20 minutes for a single value of thermal conductivity and a series of fittings using a minizing function to find the best fit thermal conductivity will be ineffective and costly.

Thus, a modification of the model must be made to ensure the fitting simulations are done in an effective and timely matter. For the thinner layers on the scale on nanometers, the step size will remain 10 nm, which result in approximately 50-100 nodal points for the nodal system. However, for the substrate layer with a thickness of 0.5 mm, the step size must be increased to ensure time-effective simulations. With a step size of 10 nm, the substrate would have approximately 50,000 nodal points. Given that the MATLAB software can handle a matrix size of up to 5,000 by 5,000 effectively, this particular approach will not work for this case. If the step size for just the substrate layer was multiplied by 50 or to 500 nm, then the number of nodal points for just the substrate would be reduced from 50,000 to 1,000. This modification helps reduce the computation time for a single run from 20 minutes to 1 minutes. Thus, gathering the correct thermal conductivity value with the best least squares will become faster and more effective.

The model takes into account the changing step size, as Δx is accounted for at each nodal point, so there is no need to adjust the model any further.

2.3 Benchmark Studies

In order to verify that our experimental setup is correct, control samples with known quantities of thermal conductivities are measured with the setup. For this purpose, two control samples were used: a n-type indium arsenide (nInAs) substrate and a gallium

arsenide growth on top of a gallium arsenide substrate. Both samples are coated with a thin gold (Au) film with a thickness of 70 nm.

The first aspect of this model is to figure out the trends when certain free parameters are varied. The two free parameters for this model are the thermal conductivity of the substrate and the contact resistance between the metal film and the substrate.

First, the free parameter of the thermal conductivity of the substrate was varied. For these experiments, the densities and specific heats of the Au film and InAs layer are assumed to be the same as bulk value. The thermal conductivity of the Au film layer depends on thickness and was found to be $134.4\ \frac{W}{m-K}$ at a thickness of 70 nm, different from the bulk value of $401\frac{W}{m-K}$. Holding the thermal contract resistance constant, the following graph was generated.

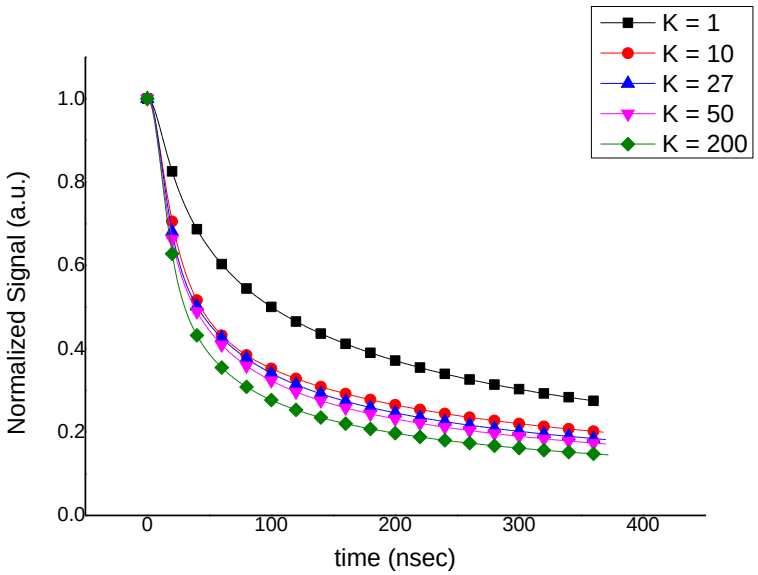

Figure 25. Sensitivity to thermal conductivity changes with everything else constant.

From Figure 10, as the thermal conductivity increases, the decay time from the normalized peak temperature to the steady state temperature decreases. This makes sense from a physical standpoint. After thermal equilibrium has been reached, the thermal energy starts diffusing away from the surface. If the substrate has a high thermal conductivity, then it should be able to conduct heat more easily and thus, the heat diffuses more quickly away from the surface, compared to other materials with lower thermal conductivities.

The next free parameter to be varied is the thermal contact resistance between the metal film and the substrate. Holding all other parameters constant, the following graph was generated.

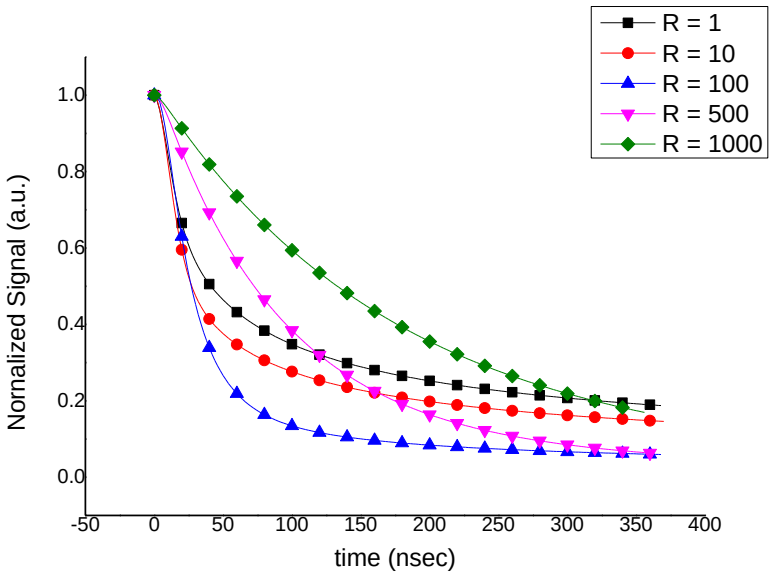

Figure 26. Sensitivity to thermal interface resistance with gold film thickness = 70 nm.

From Figure 11, there seems to be little relationship between the decay time and the thermal interface resistance. At a small interface resistance, the decay time is at an intermediate, and as the interface resistance starts to increase, the decay time decreases. However, after a certain threshold point, the decay time starts to increase with increasing interface resistance. Normally, with increasing thermal interface resistance, the decay time for the surface temperature will increase as well. However, if the thickness of the gold film is increased, then the normal relationship can be observed, as shown in the following figure.

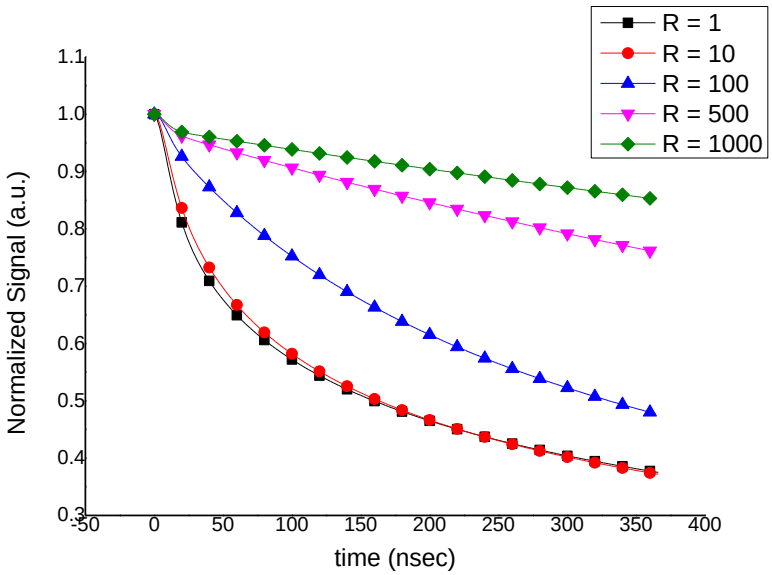

Figure 27. Sensitivity to thermal interface resistance at gold film thickness = 1 um.

From Figure 11, the decay time increases with increasing thermal interface resistance, as expected.

The behavior found in the 70-nm thin film case, however, can be explained. The definition of the heat flux across the thermal interface resistance is described with this equation:

$$q'' = \frac{\Delta T}{R_C} \tag{26}$$

where $q''$is the heat flux across the interface and R_C is the thermal interface resistance.

For the model used in these experiments, only the thin film layer absorbs all of the thermal energy from the laser. Once the thin film layer absorbs the heat, it diffuses the thermal energy throughout the subsequent layers. For thicker metal films on the scale of micrometers, the thermal energy is distributed throughout the whole layer, which results

in a lower heat flux at the interface between the metal film and the rest of the sample. For thinner films on the scale of nanometers, the thermal energy is more concentrated than that of thicker films, resulting in a higher heat flux. For small interface resistances for thin metal film case, the heat flux across the interface is high, which results in thermal energy conducting away from the surface at a faster rate. This explains the faster decay times for the thin metal films.

Now that the trends for varying each free parameter are noted, we can now check for the validity of the thermoreflectance system. First, experiments were performed to check to see if the experiment was repeatable for a single sample. After a data set was recorded, the sample was translated perpendicularly to the path of the pump beam (after decreasing the intensity of the pump beam in order to not damage the sample) in order to get a new spot.

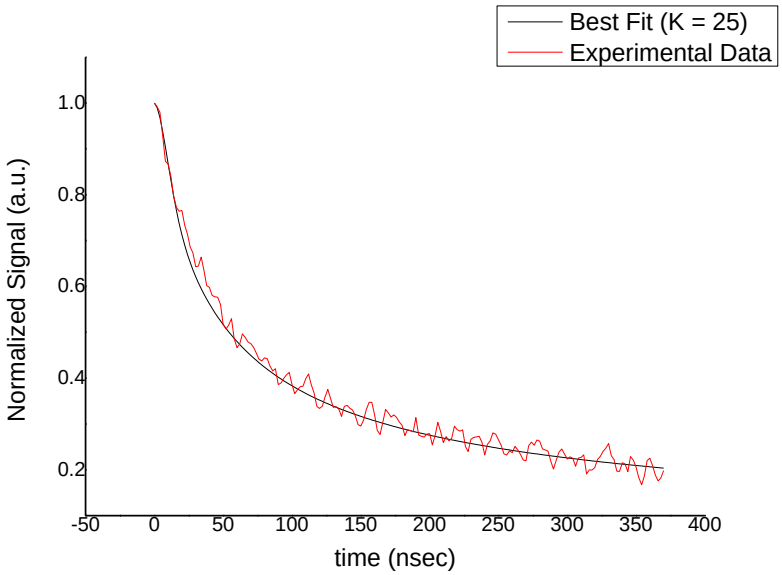

Figure 28. Thermoreflectance plot of nInAs control sample.

The bulk value of InAs is 27 $\frac{W}{m-K}$, so the measured value of 25 $\frac{W}{m-K}$ is within 10% of the bulk value. Thus, our thermoreflectance model is valid for this particular sample.

Next, the thermal conductivity for the GaAs sample was measured.

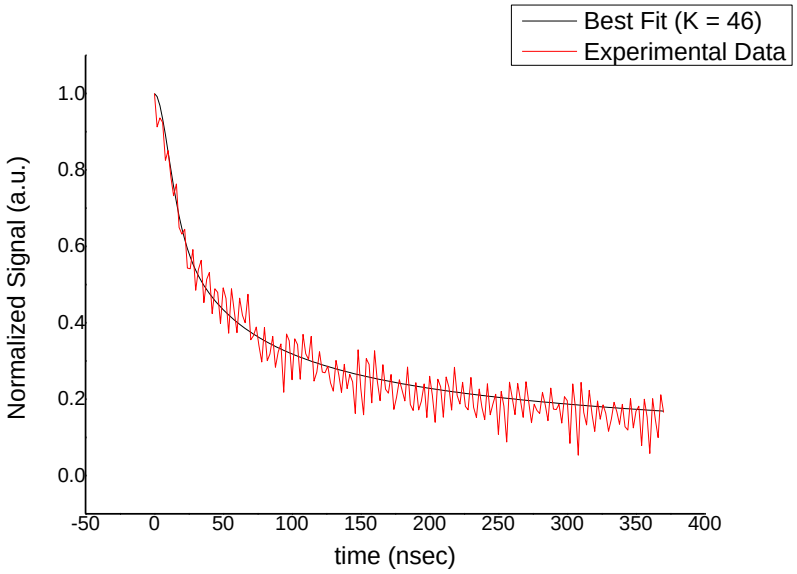

Figure 29. Thermoreflectance plot of GaAs control sample.

The bulk value for GaAs is 46 $\frac{W}{m-K}$, and the measured thermal conductivity value from the experiment was near the bulk value, so the thermoreflectance method is valid.

2.5 Summary

The thermoreflectance method is a good method to find the thermal conductivity of materials on the scale on nanometers. Using the 1-D heat conduction model with heat generation helps simplify the process to find the thermal conductivity as it eliminates any thermal conductivity dependence on the in-plane axis of the surface. Also, the

thermoreflectance method shows the dependence of the thermal conductivity and thermal interface resistance on decay time. With increasing thermal conductivity, the decay time decreases. With thermal interface resistance, it depends on the thickness of the metal film. With thicker metal films, the decay time increases with increasing thermal interface resistance. With thinner metal films, the decay time first decreases before reaching a threshold point and increasing with thermal interface resistance. The experiments were then performed on control samples and checked to see if it matched with bulk values.

Chapter Three: Case Study of Semiconductor Interfacial Misfit Arrays

3.1 Description of IMF Semiconductor Samples

The samples used in these experiments were developed and manufactured using epitaxy. Epitaxy is the act of growing crystalline structures on a crystalline substrate. This method has many applications, especially in the use of semiconductor manufacturing and nanotechnology. There are several different types of epitaxy depending on the growth conditions and materials used in the process. Homoepitaxy involves depositing a crystalline material on top of a substrate of the same material. This method is used to create materials, which have different doping levels than the bulk substrate. Heteroepitaxy involves growing a crystalline material on top of a substrate of a different material. This particular method is used to create new crystalline structures, which, otherwise, are not attainable by bulk materials.

The samples that are discussed in this paper are constructed using III-V semiconductor materials. III-V semiconductors uses materials that come from groups III and V on the periodic table (Katz 1992). Group III (or Group 13) elements include aluminum, gallium, indium, and thallium while Group V (or Group 15) elements include phosphorous, arsenic, antimony, and bismuth. The main III-V semiconductor compounds that are used for this experiment are indium arsenide (InAs), gallium arsenide (GaAs), and gallium antimonide (GaSb).

The difficulty of growing this epitaxial growths is the mismatch of the lattice constant between the two different layers. For example, a GaSb epitaxial layer on top of a

GaAs substrate, the lattice misfit is around 7.8% (Jallipalli 2007). Because of this high lattice misfit, the thread dislocation density of theses heteroepitaxially-grown crystals is high at the interface. These defects create changes in the crystal structure of the epitaxial layer, which influence the electrical and optical properties of this layer. Thus, minimization of the threading dislocation density is of utmost importance when manufacturing these materials.

One method to reduce the threading dislocation density is by adding a buffer layer between the epitaxial layer and the substrate (Jallipalli 2007). This buffer layer is used to bend the threading dislocations before the main epitaxial layers were deposited onto the substrate. The other method is to use an interfacial misfit array to reduce the strain energy caused by these threading dislocations prior to depositing the epitaxial layers. These interfacial misfit arrays reduce the thread dislocation density at the interface by laterally propagating (90°) these threading dislocations (Jallipalli 2007). From the use of the IMF arrays, the electrical and optical properties can be improved without having to use a thick metamorphic buffer layer.

With the improvement in the electrical and optical properties, the use of IMF arrays now turn to whether there was any change in the thermal properties of these materials. If there is little to change to the thermal conductivities of these materials, then the material is considered to be in high quality.

The samples were provided by Professor Seth Bank's group from the Electrical Engineering Department at the University of Texas at Austin. These samples consisted

of epitaxially grown InAs at varying growth conditions and thicknesses on top of a GaAs substrate. Figure 15 shows the general construction of these samples.

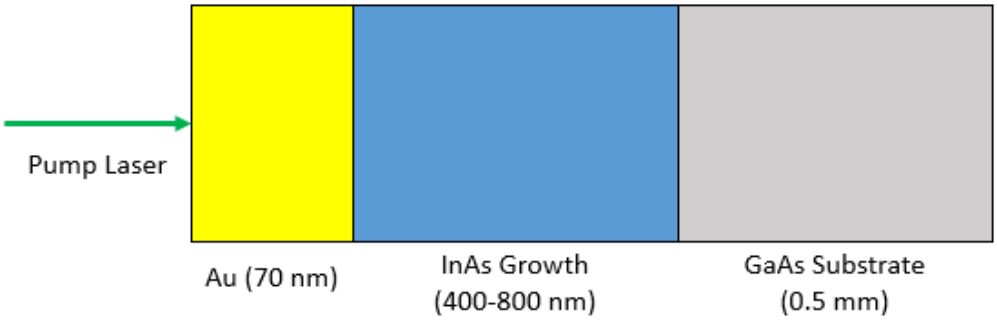

Figure 30. General schematic for the samples measured.

Modeling the nodal system for these samples will be similar to that from Chapter Two, except now, they will be three layers instead of two. Interface resistances will occur at both the gold-InAs interface and the InAs-GaAs interface.

Figure 16 below shows the construction of each sample with its corresponding layers. The numbers inside each layer represents the lengths in angstroms. Each sample is coated with a 70-nm thick metal film.

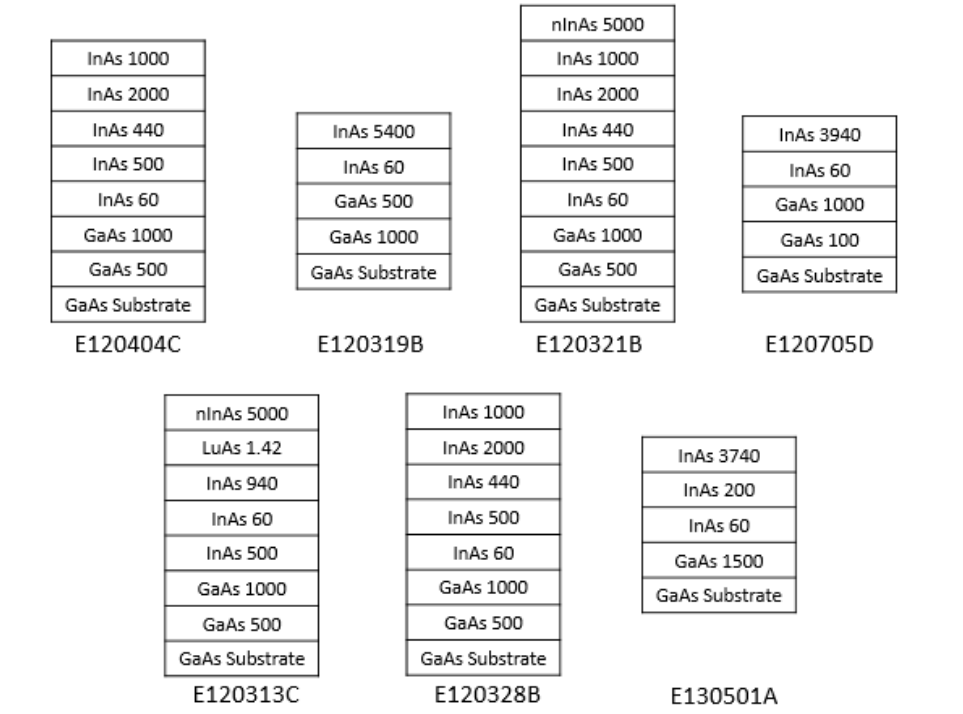

Figure 16. Schematic of the samples being measured with the units of the thicknesses of each layer in angstroms.

Seth Bank's group have measured the photoluminescence of each sample and want to know if the IMF growths affect the thermal properties of the material.

Experiments were performed on all of the samples with the experimental parameters from chapter two.

3.2 Trends of Measurements of IMF Semiconductor Growths

As before in Chapter Two, the free variables of this set are the thermal conducitivity of the unknown layer and the interface resistance. The interface resistance between the gold layer and the next layer has been discusses in chapter two, so it will not discussed here again.

First, the graphs are checked to see how they would behave with varying thermal conductivity of the growth layer. A thickness of 400 nm for the growth layer is used for this case.

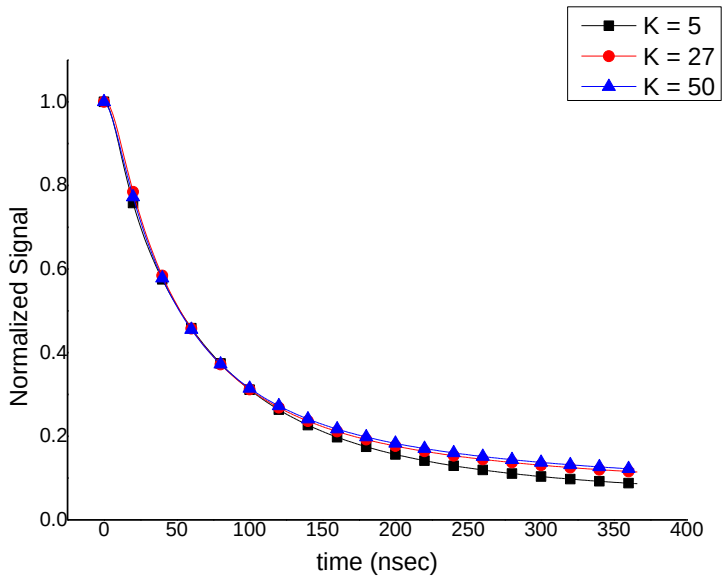

Figure 17. Sensitivity to thermal conductivity for IMF growth samples at 400 nm thickness.

From Figure 17, it seems that the decay time increases with increasing thermal conductivity, which is opposite of what is expected. Again, the thickness of the layer has to come into play, just like the case with the Au thin film thickness. Figure 18 show the behavior of the graphs if the thickness of the growth layer increased to 8000 nm.

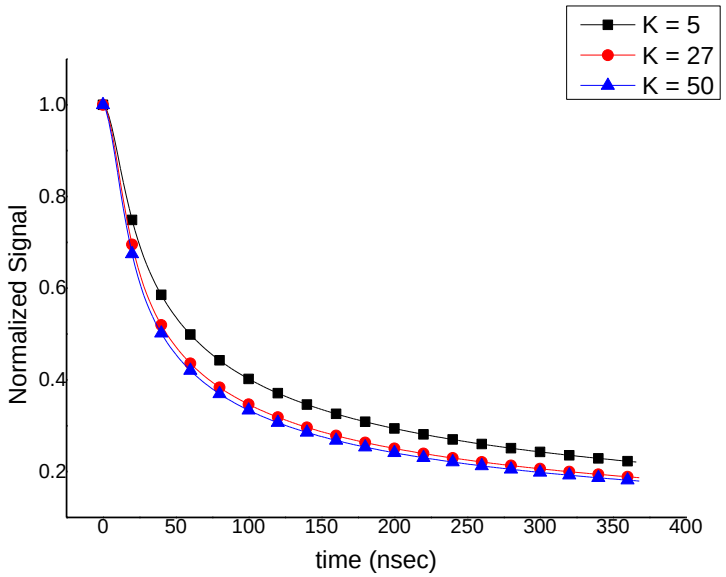

Figure 18. Sensitivity to thermal conductivity for IMF growth samples at 8000 nm thickness.

From Figure 18, the decay time decreases with increasing thermal conductivity, which is expected. Because of this, the differences in trends between Figures 17 and 18 are due to the thickness of the IMF growth layers. This can be explained visually if we treat the IMF growth layer as a contact resistance between the gold film and the substrate. Our definition of the thermal resistance is as follows:

$$R = \frac{L}{k} \tag{26}$$

where L is the thickness of the layer. Low thermal conductivities correspond to high thermal resistances, but if we increase the thickness of the layer by a factor of 20, then the resistances become much smaller.

The interface resistance between the growth layer and the substrate is then varied and checked for trends.

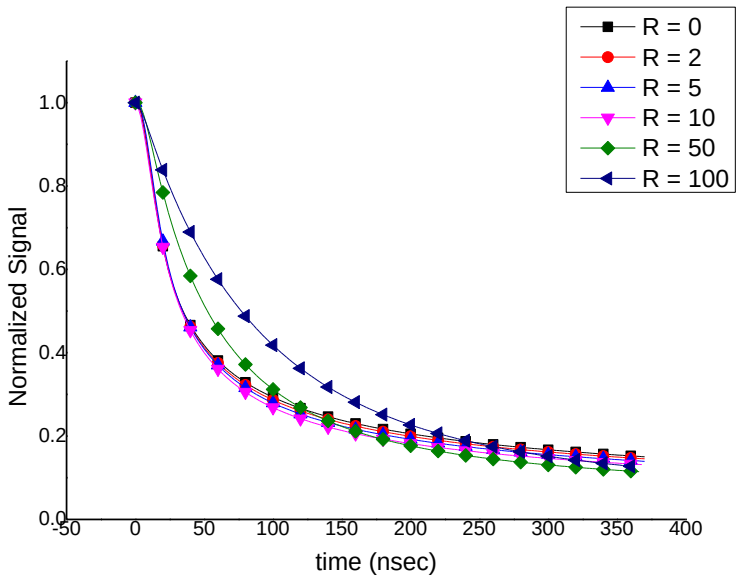

Figure 19. Sensitivity to thermal interface resistance between IMF growth and substrate layers.

From Figure 19, it seems that the decay time decreases with increasing interface resistances, though at small resistances. Then, at a threshold point, the decay time starts to increase with increasing thermal interface resistance. Thickness of the layers do play a factor in the behavior of the decay time, and since the threshold point is relatively low than the other cases, it is safe to assume that the behavior is normal.

3.3 Experimental Results

Now that the general trends for the IMF semiconductor growths have been noted, it is time to perform experiments and find the thermal properties of these samples.

First, in order to verify that the samples can be used in this setup, a set of control samples was measured. This was covered in the previous chapter with the two samples: a n-type indium arsenide (nInAs) substrate and a gallium arsenide growth on top of a gallium arsenide substrate. Both samples produced data that outputted thermal

conductivities close to the bulk literature value. Because of this, we can proceed and perform experiments on the experimental samples.

Each experiment was performed 3 to 5 times on each sample, and the output signals were averaged in order to reduce the noise of the data. Table (#) shows the results of each sample with the corresponding interface resistance.

Sample	**InAs Layer Thickness (nm)**	**Thermal Conductivity (W/m-K)**	**Interface Resistance Between Metal and Growth (m^2-K/W)**	**Interface Resistance Between Growth and Substrate (m^2-K/W)**
E120404C	400	10.68	5	47
E120319B	546	19.25	5	35
E120321B	800	14.6	2	11
E120705D	400	6.64	4	46
E120313C	750	17.9	2	47
E130328B	400	9.43	2	46
E130501A	400	24.5	6	45

Table 1. Thermal conductivity and interface resistance results

From Table 1, most of the samples have thermal conductivities that are different from the given bulk value of 27 $\frac{W}{m-K}$. It is a possibility that the growth conditions of each sample could have affected the crystal structure of InAs, which resulted in the reduction of the thermal conductivity.

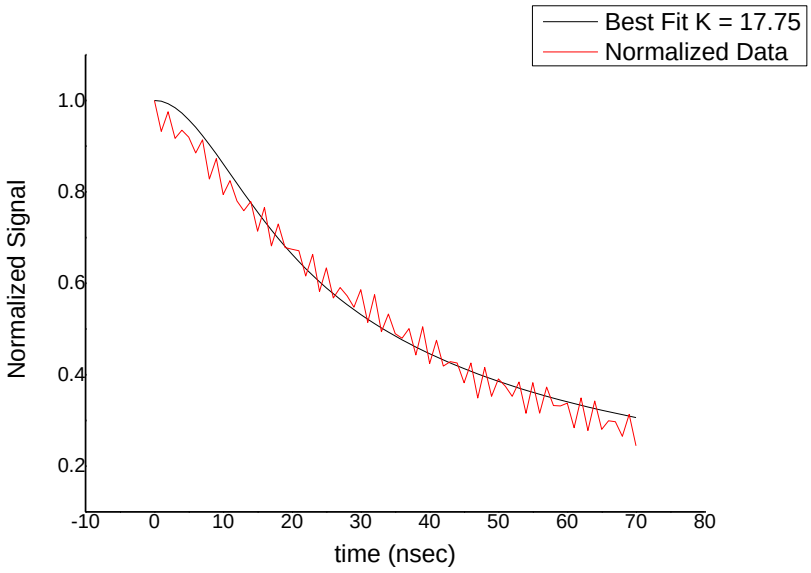

Figure 20. Thermoreflectance plot of sample E120319B

With these experimental results, we can compare them to the photoluminescence results, acquired by Dr. Seth Bank's group prior to these measurements. Photoluminescence is an optical property where light is emitted after a material absorbs photons. A high photoluminescence is associated with a high quality crystal with a low density of defects. Figure 20 shows the relationship between photoluminescence and thermal conductivity.

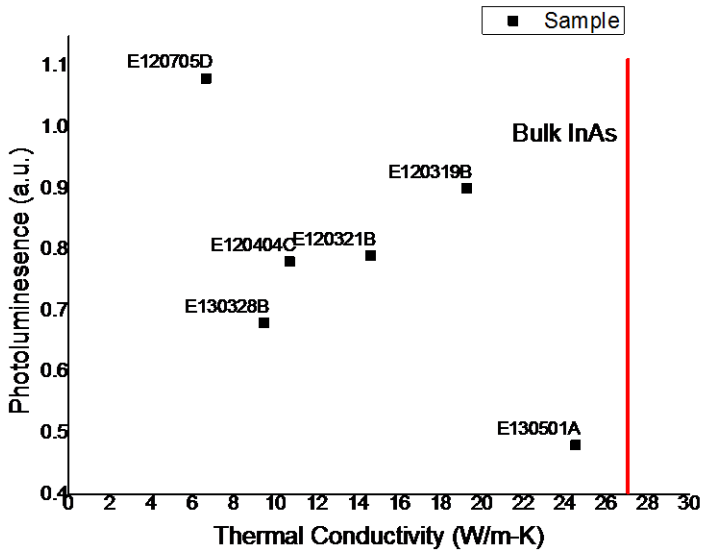

Figure 21. Photoluminescence vs. Thermal Conductivity plot

From Figure 21, there seems to be downward trend relating the photoluminescence and thermal conductivity. With increasing thermal conductivity, the photoluminescence decreases. This is interesting with the fact that a high photoluminescence indicates a high quality crystal with little defects. Because the defects are at a low density, the mobility of electrons should be higher and thus, the thermal conductivity should be higher.

Another thing to note is the interface resistance between the InAs growth layer and GaAs substrate and the thickness of the growth layer. The purpose of the interfacial misfit arrays is to reduce the lattice mismatch between two materials. The effects that it has on the thermal conductivity of the growth layer are unknown. However, looking at Figure 21, there is a notable relationship between the thickness of the InAs growth layer and the thermal interface resistance. With increasing InAs growth layer thickness, the

thermal interface resistance between the growth layer and substrate decreases. This phenomenon can explained due to the nature of interfacial misfit arrays.

As mentioned before, the purpose of the interfacial misfit arrays is to propagate any threading dislocations laterally in the sample. From a physical standpoint, a thicker InAs growth layer would allow these threading dislocations more space to propagate. Thus, the defects at the interface would less in number and would result in a lower thermal interface resistance.

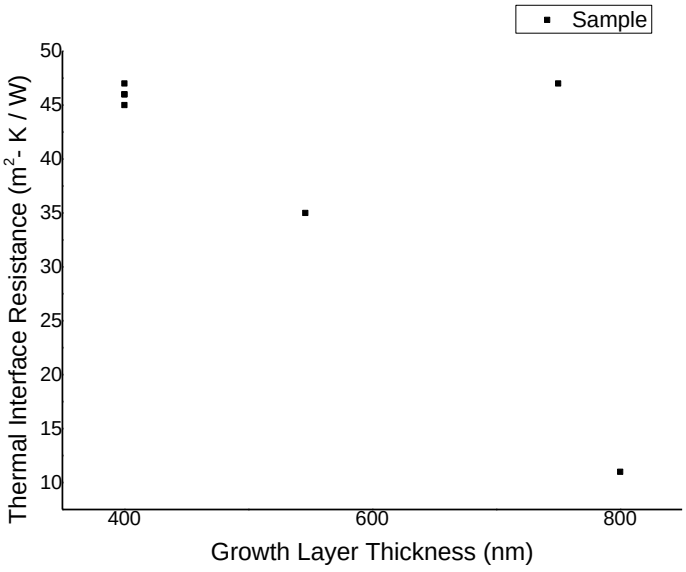

Figure 22. Thermal Interface Resistance vs. Growth Layer Thickness plot

The exception to this thought is the sample E120313C, which has an InAs growth layer thickness of approximately 750 nm. The best fits showed that the thermal interface resistance between the growth layer and the substrate is comparable to the samples whose growth layer thicknesses are at 400 nm. However, an explanation for this has to do with the construction of the InAs growth layer of that particular sample. In that sample, a layer

of lutetium arsenide (LuAs) nanoparticles was added into the growth layer, about 570 nm deep from the front surface of the sample, which leaves about a distance of 250 nm between the substrate and the nanoparticle layer. This could explain why the thermal interface resistance for this particular sample is high, relative to its InAs growth layer thickness. The lateral propagations of the thread dislocations ended at where the LuAs nanoparticles are located. Thus, the dislocations are more localized around this area between the LuAs nanoparticles and the substrate, which leads to a higher thermal interface resistance between the InAs growth layer and the GaAs substrate.

3.5 Summary

A look at IMF semiconductor growths was performed to see the benefits of such a technique. IMF growths help reduce the strain energy on a semiconductor by propagating the threading dislocations laterally. Therefore, the electrical and optical properties, such as photoluminescence, are improved for these materials. Experiments were then performed to see if the thermal properties were affected, due to the IMF arrays. From the experimental results, it seems that thermal conductivity has decreased with increasing photoluminescence. Another trend noted was the relationship between the IMF growth layer thickness and thermal interface resistance between the IMF growth layer and the substrate. As the IMF growth layer increases, the thermal interface resistance between the IMF growth layer and the substrate decreases. This relationship is due to the nature of the IMFs. These IMFs propagate the threading dislocations laterally from the interface, and having a thicker layer would help distribute the dislocations more through the growth

layer. The exception is the sample with LuAs nanoparticles embedded inside the IMF, which has a thermal interface resistance comparable of that to other samples with thinner IMF growth layers. Though, this can be explained due to the dislocations possibly ending at the nanoparticle layer and the dislocations having a smaller volume to distribute. Further work will be needed to determine whether these effects hold true.

Chapter Four: Summary and Future Work

4.1 Summary

Today's electronic devices are performing at high capacities with them generation more power and running at faster speeds. They are also getting smaller on the scale of nanometers which allow more portable usage. However, with these higher capacities come greater challenges to help keep device cool. That is why the thermal properties of these materials must be known. Many methods and techniques were developed throughout the years in order to find out these thermal properties, starting with the steady state bar method and going to more complex and faster like the thermoreflectance method. With these faster methods, thermal properties of new materials can be discovered in a relatively short amount of time.

The thermoreflectance method is a useful method to determine the thermal conductivities of materials. Many different types of setups exist in order to implement this method. The method used in this paper uses two laser sources: one as a heat source and one to probe the changes in reflectivity due to the heat source. Two control samples, an n-type InAs substrate and a GaAs substrate, were used to see if the experimental setup was valid. Both were coated with a 70 nm Au metal film. Because the samples were cleaned in an acid bath before applying the gold metal film, it was assumed that the thermal interface resistance was close to zero. After the experiments were performed, it was found that the measured thermal conductivity for both samples fall within 10% of the bulk thermal conductivity from literature.

Interfacial misfit (IMF) arrays help reduce the strain energy of a device by laterally propagating the threading dislocations laterally. Therefore, the electrical and optical properties of these materials can be improved. Experiments were done to see if the thermal properties were affected, due to the IMFs. After experiments were performed, it was found that with increasing photoluminescence, the thermal conductivity decreased. There was also a relationship between the IMF growth thickness and the thermal interface resistance between the IMF growths and the substrate. With increasing InAs growth layer thickness, the thermal interface resistance between the growth layer and substrate decreases.

4.2 Future Work

Although the experimental setup was valid, there are always ways to improve it. More accurate ways to align the pump and probe beam spots on the sample can be added to the system, such as a CCD camera. The pump to probe beam spot size ratio can also be improved by introducing appropriate optical elements which change the size of either the pump or probe beam spots.

For the IMF arrays, new samples could be manufactured to see the effects of the thickness of the IMF growths have an effect on thermal conductivity and thermal interface resistance. Some of the experimental data showed that there is a relationship between the thickness of the IMF growth layer and the thermal interface resistance, so further work will be needed to study this effect. It is quite possible that the effect of the thermal interface resistance could affect the thermal conductivity measurements, so having thicker IMF growths could reduce that effect.

Appendix A. Properties of Materials

Table A-1. Properties of materials used in thermal fittings

	Density (kg/m^3)	Specific Heat (J/kg-K)	Thermal Conductivity (W/m-K)
Si[1]	2330	712	149
Au[1]	19300	129	134.4*
InAs[2]	5670	248	27
GaAs[2]	5320	338	46

*Thermal conductivity measured at thickness of 70 nm.

[1]Goldsmith 1961
[2]Katz 1992

Table A-2. Optical Properties of Materials

	Wavelength (nm)	Refractive Index (real)	Refractive Index (imaginary)	Absorption Coefficient (cm^{-1})
Au	532	0.54410	2.1404	$5.0559*10^5$
	632	0.19681	3.2478	$6.4578*10^5$

Source: Rakic, 1998

References

Goldsmith, A., Waterman, T. E., Hirschhorn, H., J. (1961) *Handbook of thermophysical properties of solid material* (Vols. 1,2) New York, New York: The MacMillan Company.

Incropera, F. P., DeWitt, D. P., Bergman, T. L., Lavine, A. S. (2007). *Fundamentals of Heat and Mass Transfer*, 6th Edition. Danvers, Ma: John Wiley & Sons, Inc.

Jallipalli A., Balakrishnan G., Huang S. H., Khoshakhlagh A., Dawson L.R. & Huffaker D.L. (2007). Atomistic modeling of strain distribution in self-assembled interfacial misfit dislocation (IMF) arrays in highly mismatched III–V semiconductor materials. *Journal of Crystal Growth*, 303,449–455

Katz, A. (1992). *Indium phosphide and related materials : processing, technology, and devices*. Norwood, Ma: Artech House, Inc.

Laubitz, M. J. (1984). Axial heat flow methods of measuring thermal conductivity. Maglic, K. D., Cezairliyan, A. & Peletsky, V. E. (eds), *Compendium of Thermophsyical Property Measurement Methods, 1.* New York: Plenum Press.

Magnes J., Odera D., Hartke J.. Fountain M, Florence L., and. Davis V. (2006). Quantitative and Qualitative Study of Gaussian Beam Visualization Techniques. http://arxiv.org/abs/physics/0605102.

Parker, W. J., Jenkins, R. J., Butler, C. P. & Abbott, G. L. (1961). Flash method of determining thermal diffusivity, heat capacity and thermal conductivity. *Journal of Applied Physics*, 32(9), 1679-1684.

Rakić A. D., Djurišic A. B., Elazar J. M., & Majewski M. L. (1998). Optical properties of metallic films for vertical-cavity optoelectronic devices, *Appl. Opt.*, 37, 5271-5283

Schelling P.K., Shi L. & Goodson K.E. (2005). Managing heat for electronics. *Materials Today*, 8(6), 30-35

Ujihara, K. (1972). Reflectivity of materials at high temperatures. *Journal of Applied Physics*, 453(5), 2376-2383.

Vita

Khai Ta Nguyen was born in Houston, Texas. He graduated from J. Frank Dobie High School, Houston, Texas, in 2009 and enrolled in Rice University in Houston, Texas that year. After graduating from Rice University with a Bachelor's of Science in Mechanical Engineering with Cum Laude honors in May 2013, he entered the graduate program in the Mechanical Engineering Department at the University of Texas at Austin in August 2013.

Permanent Address: 10422 Chelseabrook Ln.
Houston, TX 77089